Urban flood numerical modeling and hydraulic performance of a drainage network: A case study in Algiers, Algeria

El khansa Lameche[a], Hamouda Boutaghane [iD][b,*], Mohamed Saber[c], Karim I. Abdrabo[d], A. Malek Bermad[e], Messsoud Djeddou[f], Tayeb Boulmaiz[g], Sameh A. Kantoush[c] and Tetsuya Sumi[c]

[a] Faculty of Science and Technology, Department of Hydraulics, Larbi Ben M'hidi University, Oum El Bouaghi, Algeria
[b] Soils and Hydraulic Laboratory, Badji Mokhtar – Annaba University, P.O. Box 12, 23000 Annaba, Algeria
[c] Disaster Prevention Research Institute (DPRI), Kyoto University, Kyoto 611-0011, Japan
[d] Department of Urban Management, Graduate School of Engineering, Kyoto University, Kyoto 611-0011, Japan
[e] Department of Hydraulics, Ecole Nationale Polytechnique, El harrach – Algiers, Algeria
[f] Research Laboratory in Subterranean and Surface Hydraulics (LARHYSS), Faculty of Sciences and Technology, Mohamed Khider University, Biskra, Algeria
[g] Materials, Energy Systems Technology and Environment Laboratory, Ghardaia University, Ghardaia, Algeria
*Corresponding author. E-mail: boutaghane.hamouda@univ-annaba.org

[iD] HB, 0000-0002-8260-0397

ABSTRACT

Urban sewer system management is challenging due to its higher vulnerability to flooding caused by rapid urbanization and climate change. For local decision-makers, storm water management is essential for urban planning and development. Therefore, the main objective of this study is to develop a numerical model for the sewerage network of the central catchment area of Algiers since it has experienced frequent overflows during the winter season. For this purpose, to model the sewerage networks, the model was built by coupling ArcGIS with MIKE URBAN. Its calibration and validation were performed using real-time measurements with a time step of 15 min. The model was evaluated by several statistical indicators, such as the coefficient of determination (R^2), Nash–Sutcliffe efficiency (NSE), root mean square error (RMSE), and percent bias (PBIAS). The model results showed acceptable model performance, with an NSE superior to 0.50, R^2 of approximately 0.63, RMSE of 7%, and PBIAS of 10% during the validation of the model. The performance parameters prove the reliability of the developed model. The employed model can be applied in other regions and could be helpful for policymakers and managers to improve flood mitigation measures based on the model prediction of the sewerage network.

Key words: climate change, flood mitigation, flood vulnerability, Mike Urban MOUSE, policymakers, urban sewer systems

HIGHLIGHTS

- Facilitate management by utilizing modeling to protect people and their property.
- Ensure that decisions are made promptly within the framework of emergency response plans in case of an alert.
- Develop a reliable digital model for studying the impact of climate change on the rainwater drainage system. Haut du formulaire.

1. INTRODUCTION

Climate change poses a significant global challenge, leading to changing rainfall patterns, increasing urbanization, and population and economic growth in flood-prone areas. This combination of factors raises the risk of urban flooding in various parts of the world (Hemmati *et al.* 2020). The hydrological cycle has been greatly affected by climate change, population growth, and urban expansion, resulting in the expansion of impervious surfaces (Morita 2011; Lee *et al.* 2015; Gigović *et al.* 2017). Urban flooding is a critical issue worldwide due to factors such as intense rainstorms, decreased permeability of urban areas, increased surface catchment volume, and inadequate drainage infrastructure. Consequently, numerous cities experience significant flood-related damages and losses each year (Xu *et al.* 2023).

Flooding has emerged as a global problem that requires immediate attention due to its harmful impacts on communities and infrastructure (Peña-Guzmán *et al.* 2017). The study of flood protection and urban water management has gained significant momentum recently, highlighting the importance of effective flood mitigation strategies (Hettiarachchi *et al.* 2017;

Zahmatkesh *et al.* 2019; Loudyi & Kantoush 2020; Tamiru & Wagari 2021). Arid countries, including Arab countries, are particularly susceptible to frequent and devastating flooding events due to approximately one-third of global land being classified as arid or semiarid and nearly 20% of the world's population residing in these regions (Dahm *et al.* 2002; Youssef *et al.* 2015; Ahmed 2019; El-Kholei 2019).

The hydrological cycle has undergone significant changes in Arab countries due to climate change, population growth, and urban expansion, resulting in the proliferation of impervious surfaces (Morita 2011; Lee *et al.* 2015; Gigović *et al.* 2017). In these countries, the issue of urban flooding is exacerbated by unsustainable horizontal and vertical densification, which puts additional strain on ageing sewerage networks that were not designed to handle increased flow during extreme events (Abdrabo *et al.* 2021). Moreover, rapid urban growth and inadequate land-use planning have led to the emergence of impoverished neighborhoods lacking essential housing, infrastructure, and services, making vulnerable populations, especially women and children, more susceptible to flood hazards (Abdrabo *et al.* 2020, 2022a, 2022b; Saber *et al.* 2020). The lack of comprehensive knowledge about floods further complicates flood management and forecasting efforts (Abdelkarim *et al.* 2019; Nkwunonwo *et al.* 2020; Salazar-Briones *et al.* 2020).

Algeria, the largest country in Africa with diverse climate zones, including a mild Mediterranean coastal climate, a semiarid zone called the High Plains, and the arid Sahara desert in the south, faces significant natural disaster risks, with floods accounting for the majority of recorded hazards between 1980 and 2010 (World Bank 2014). Floods cause casualties, damage to buildings, and disruptions to roads and urban infrastructure in Algeria (Sardou & Missoum 2016; Hamlat *et al.* 2021). Flash floods in Algeria are characterized by their short duration, limited spatial extent, and high flood peaks. The country has witnessed major flood events resulting in substantial human and material losses in various regions, such as the devastating floods in Algiers in 2001, the catastrophic floods in the valley of Oued M'zab in 2008, and the floods in Annaba in 2010, as well as more recent floods in Oum el Bouaghi, Constantine, Chlef, Jijel, and Algiers in 2018 and 2021 (Sardou & Missoum 2016).

Traditionally, rainwater management in Algeria relies on recorded extreme events, but accurately predicting sewerage network discharges remains a challenge due to the lack of powerful tools for flood prediction (Zhou *et al.* 2013). While several modeling studies have been conducted on wadi flooding in Algeria, detailed studies on the sewage system are lacking (Boutaghane *et al.* 2021). Similarly, research in other arid countries has predominantly focused on river flooding, resulting in limited understanding of urban sewerage systems (Youssef *et al.* 2015; Lefebvre *et al.* 2019; El Khalki *et al.* 2020; Farooq & Alluqmani 2021). Existing network modeling studies often rely on daily data, neglecting sub-hourly variations and real-time monitoring capabilities (Talchabhadel & Man Sharkya 2015; Hermoso *et al.* 2018; Tamiru & Wagari 2021).

To address these limitations and provide a comprehensive approach to flood management in Algerian urban areas, it is necessary to explore advanced modeling techniques that consider both wadi and sewerage systems. This approach would enable accurate predictions and actionable insights for flood dynamics, leading to effective flood risk management strategies and the resilience of urban areas. In this study, we propose the utilization of the MIKE URBAN MOUSE numerical modeling tool, which leverages actual sub-hourly measurements at the sewerage network level. This approach represents a significant advancement in flood management in Algeria as it considers real-time data and captures the complexities of both wadi and sewerage systems.

The proposed approach offers several unique features and advantages compared to existing methods. Firstly, by integrating sub-hourly measurements, it captures the temporal variability of flow and precipitation, allowing for a more accurate representation of flood dynamics. This real-time monitoring capability enables proactive flood management and timely decision-making. Secondly, the incorporation of the MIKE URBAN MOUSE model, a well-established and widely used tool in previous studies, enhances the credibility and practicality of the proposed modeling approach (Lee *et al.* 2015; Bisht *et al.* 2016; Nguyen *et al.* 2020). The extensive application of this model provides a solid foundation for its implementation in the context of Algerian urban areas.

The proposed approach also addresses the limitations of previous methods by considering both wadi and sewerage systems, providing a more comprehensive understanding of flood dynamics in urban areas. Additionally, the sub-hourly resolution of data enables the identification of rapid fluctuations in flow patterns and their impact on urban infrastructure. This level of detail is crucial for designing and implementing effective flood mitigation strategies tailored to the specific characteristics of Algerian urban areas.

In summary, this research aims to fill existing knowledge gaps and provide a robust framework for flood management in urban areas of Algeria. By utilizing advanced modeling techniques and leveraging sub-hourly measurements, the study seeks

to empower stakeholders with the necessary tools and insights to mitigate the impacts of flooding, enhance urban planning practices, and foster sustainable development in the face of increasing climate challenges. The proposed utilization of the MIKE URBAN MOUSE model, based on actual sub-hourly measurements, represents a significant advancement in flood management in Algeria, facilitating the development of a reliable and operable model for proactive decision-making. This research contributes to the field by addressing the limitations of previous methods and providing

2. STUDY AREA SELECTION

The capital city of Algeria has encountered devastating floods characterized by their brief duration and high intensity, which is a common occurrence in Mediterranean regions (Lefebvre *et al.* 2019; El Khalki *et al.* 2020; Loudyi & Kantoush 2020; Stefan *et al.* 2021). Among the numerous flood events in Algeria, the Bab el Oued floods in November 2001 left an indelible mark on the collective memory of Algerians. This catastrophic event resulted in an estimated loss of 900 lives (Boutaghane *et al.* 2021), prompting the authorities to initiate various flood protection projects and researchers to embark on extensive research endeavors in flood mitigation.

The capital city of Algeria, Algiers, covers an approximate area of 770 km^2. A significant portion of the rainfall that enters the sewerage system in Algiers originates from the Bouzareah Massif. This massif, though only partially urbanized, comprises multiple wadis that drain the upstream region of the catchment area. Frequently, these wadis join the sewerage collector's downstream, carrying substantial flows. The sewerage network in Algiers primarily consists of unitary types, except for specific areas with separated or pseudo-separated systems, which were established during the colonial era.

The collection network in the Wilaya of Algiers follows a branching pattern and largely relies on gravity flow, owing to the favorable topography. However, the Bab Ezzouar – Dar El Beida sector, situated in a basin that was formerly a marshland, lacks a natural outlet, necessitating the pumping of collected water (both wastewater and rainwater) to the Oued Smar. Conversely, the transfer of sewage to treatment plants typically involves the use of pumping stations.

The sewerage system in Algiers consists of infrastructure built at different periods. Some collectors, primarily in the Kasbah area, date back to the Turkish period and are still in use. The network was further expanded during the colonial period (1830–1962), and additional construction has taken place since Algeria gained independence. In Algiers, there are around 20 rain gauges that provide daily data, along with nine stations recording rain data every 15 min (Figure 1).

The sewerage network of Algiers comprises three main watersheds: east, center, and west. Our research focuses on studying the central watershed, which requires updates due to frequent overflows. This region has a dense hydrographic network, characterized by numerous secondary tributaries and spanning a linear distance of approximately 600 km. The primary wadi of interest in our study area is Oued El-Harrach. The central region includes several wadis and tributaries that significantly contribute to the sewerage network overflows at their interaction points.

The total length of the sewerage network in Algiers is estimated to be 3,780 km, including 318 km of the main network, with 161 km being visitable ($D \geq 1{,}500$ mm at 1,600 mm). The model used for this study was primarily developed by the Algiers Water and Sewerage Company using the MOUSE software. The model consists of ten storage basins, 357 sub-basins, eight lifting stations, 87 spillways, around 30 outlets, 1,788 maintenance holes, and 1,788 pipes of various shapes.

3. METHODOLOGY AND DATA PROCESSING

3.1. Processing rainfall data

Hydrological simulation plays a crucial role in predicting flood occurrences for a given return period (Hingray *et al.* 2014) and quantifying damages by identifying vulnerable areas. The fundamental component for hydrological studies and simulations is rainfall measurement. Typically, rainfall data are presented as a 24-h time series published by meteorological services (Meylan & Musy 1999).

Intensity–Duration–Frequency (IDF) curves have been extensively studied by researchers, who have proposed various mathematical or empirical approaches (Bell 1969; Chen 1983; Chow *et al.* 1988). IDF curves are essential in the field of flooding as they synthesize data collected over a long period and aid in sizing sewerage network structures, particularly special structures for point flow estimation. Furthermore, IDF curves are used to determine project rainfall, which serves as input data for hydrological modeling (Chocat 1997; Musy & Higy 2010).

Different equations are employed in hydrology, such as Gauss, Gumbel, Galton, and Fréchet (Laborde 2000). The Generalized Extreme Value (GEV) distribution is used to model the Annual Maxima Series (AMS) (Hosking 1997). Various
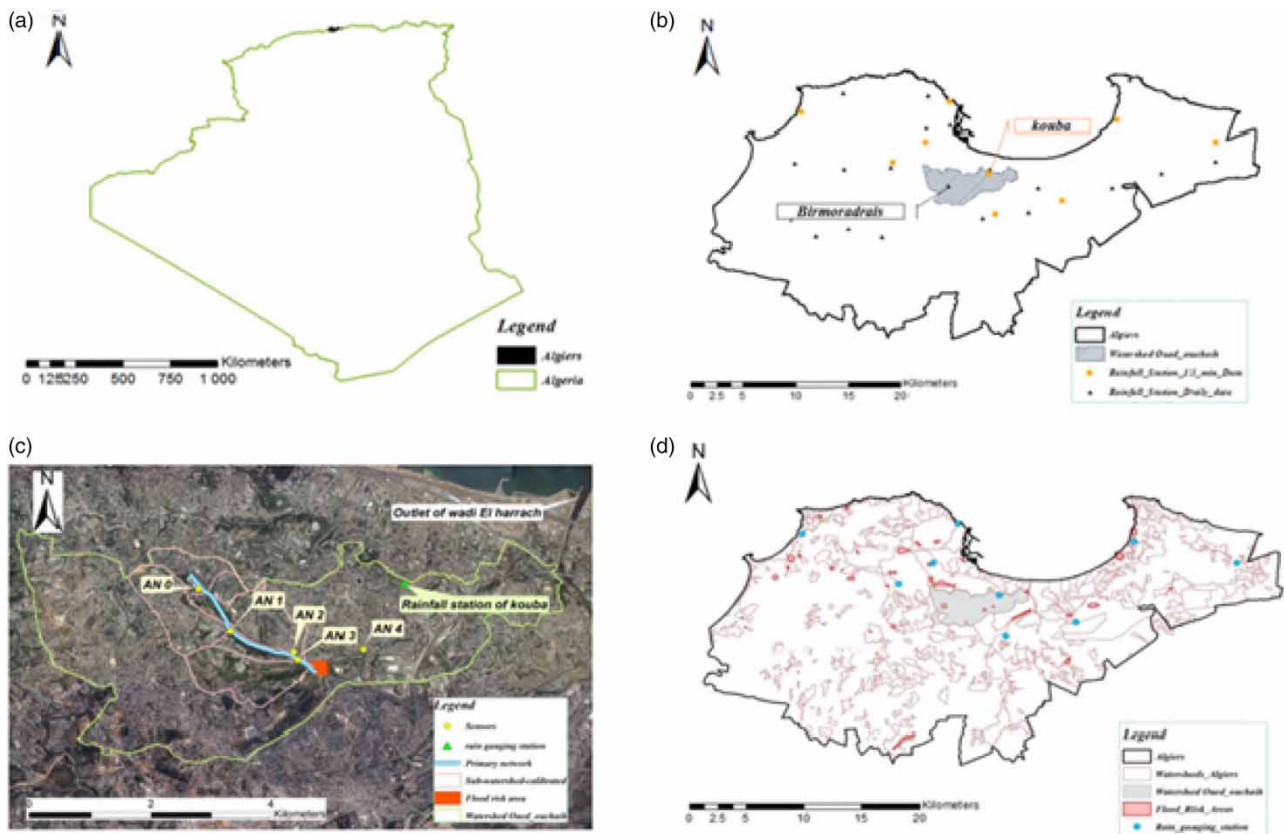
Figure 1 | The location maps show the study area in northern Algeria (a), rainfall stations (b), sub-catchments (c), and the pilot study area (d).

researchers have explained and detailed the different equations used for fitting the GEV law to AMS (e.g., Faridah *et al.* 2013). Several studies have shown that the GEV distribution is more suitable for developing AMS compared to other commonly used distributions like Gumbel (Faridah *et al.* 2013). Hence, the GEV distribution was preferred for this study.

In this study, despite rainfall data being available daily from the Bir Mourad Rais station and every 15 min from the Kouba station, the Bir Mourad Rais station was selected due to its long precipitation series. Additionally, the Bir Mourad Rais station's location within the Oued Ouchaih watershed (Figure 1(b)) makes it the most representative station for the central watershed of Algiers. The entire sewerage network of this primary catchment is illustrated in Figure 2. The rainfall data covers a long period of approximately 53 years, from 1951 to 2013 (Figure 3). The AMS was derived from the complete series by selecting the maximum intensity for each year, ensuring independence and a sample size equal to the number of years observed. The GEV equation was used as the fitting law, and the Kolmogorov–Smirnov equation was used to assess the goodness of fit for the obtained series and estimate quantiles. After constructing IDF curves for different return periods (Figure 4), projected rainfall was determined for two return periods: 10 years and 100 years (Figure 5). These projected rainfall values were used to simulate the evacuation of precipitation for the 10-year and 100-year return periods across all sewerage networks of Algiers (Figure 2).

In this section, the double triangular project rainfall for the 10-year and 100-year return periods is determined using Montana's law. The parameters of the formula for the 100-year return period are obtained after constructing the IDF curves (Chocat 1997; Bertrand-Krajewski 2006). Two project rainfalls were generated for the simulations, representing rainfall events with return periods of 10 and 100 years. These rainfall events had duration of 4 h, with an intense period of 15 min, as illustrated in Figure 5.

3.2. Selection of rainfall-flow data events

In the central watershed of Algiers, there are approximately 15 height measurement sensors and six rainfall stations. Unfortunately, several sensors were lost during heavy rains, and others have experienced periodic malfunctions, resulting in gaps in
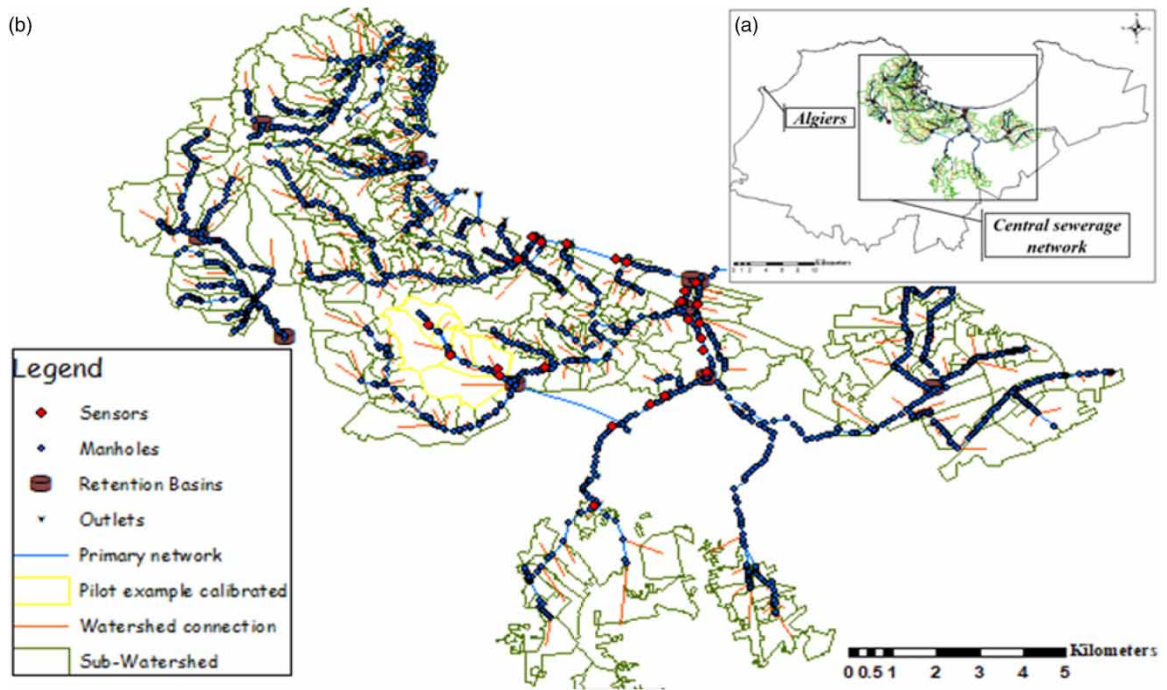
Figure 2 | Location maps depicting the central sewerage network of Algiers (a) and the central sewage network of Algiers (b).
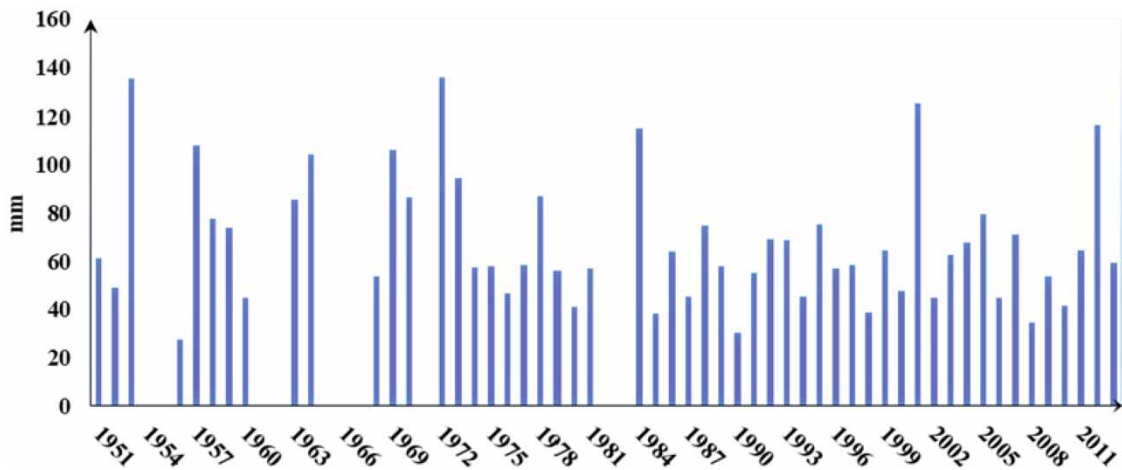

Figure 3 | Peak daily rainfall recorded at Bir Mourad Rais.

the records of water level variations. The availability of data determines the selection of sensors in the central watershed of Algiers. This research focuses on studying the Oued Ouchaih sub catchment, which is known for its sensitivity to extreme rainfall and has a higher number of functioning rain gauges and sensors, ensuring more reliable measurements. Among the six existing stations, the rainfall data from Kouba station were utilized. The records of rainfall-flow variations were captured at a time interval of 15 min.

The presented results below depict a specific sub-watershed in Ain Nadja. This sub-basin serves as an illustrative example for explaining our research strategy, although it represents only a small part of the entire study area. The water flows were measured using sensors that captured the water level variations between November 2015 and January 2020. Events were selected based on continuous functioning of the sensors for a specific period. In our example, out of the five sensors
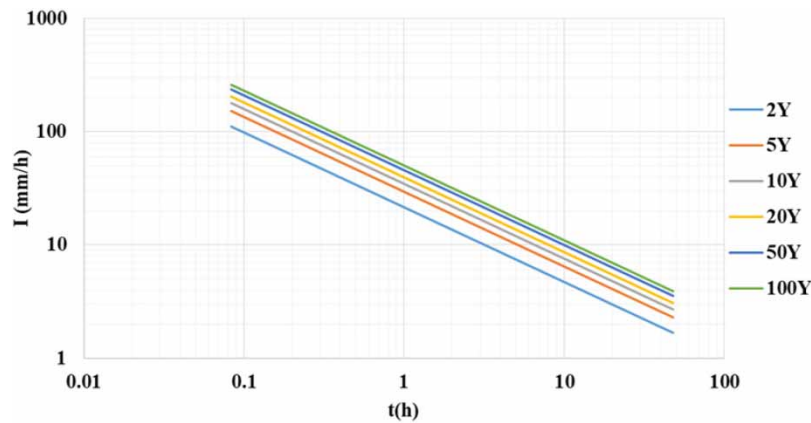
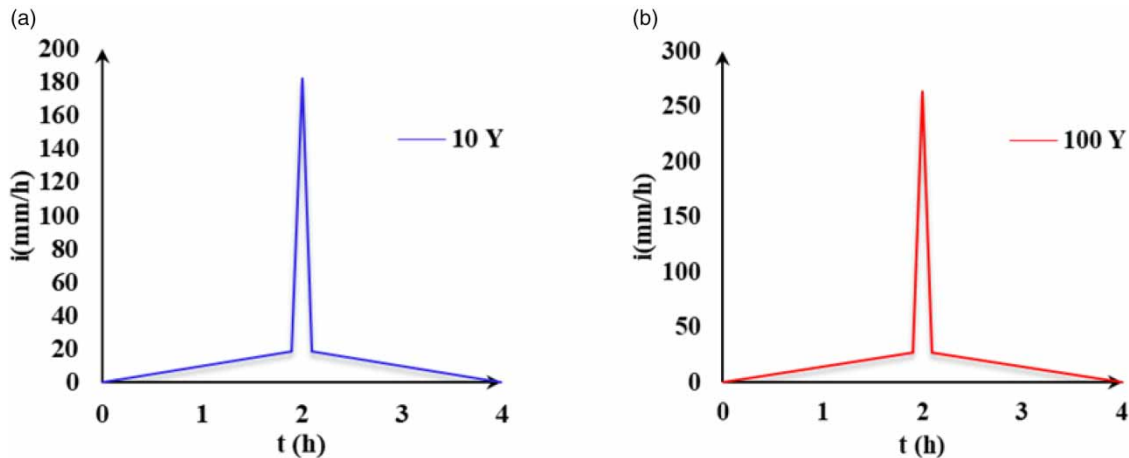**Figure 4** | IDF curves of Bir Mourad Rais.

Figure 5 | Double triangular project rainfall of Bir Mourad Rais. (a) For the 10-year return periods and (b) for 100-year return periods.

(AN0, AN1, AN2, AN3, and AN4), only AN1 and AN3 provided reliable measurements. The pilot example showcases a main network with a diameter of 1 m and 18 storm overflows (refer to Figure 1).

The choice of using the Kouba rain gauge is justified by its optimal location in relation to the sensors in Ain Nadja (the closest station) and the availability of rainfall records at a 15-min time interval. The selected events along with their cumulative rainfall are presented in Table 1.

3.3. Model construction: 'Process modeling'

In recent years, the development of decision support tools that integrate technical and economic designs has gained significant attention (El Khalki *et al.* 2020). Numerical models have been recognized as effective tools to address engineering and expert challenges. By combining software and other approaches, it becomes possible to quickly predict different trends or scenarios (Peña-Guzmán *et al.* 2017). In the water field, these models contribute to the formulation of policy strategies (Nguyen *et al.* 2020) by evaluating various proposed alternatives to solve hydraulic problems (Brendel *et al.* 2021) and assisting decision-makers in managing urban areas, which are often complex due to the network intricacies in municipalities (Löwe *et al.* 2017). Several commercially and non-commercially available software packages with varying complexity simulate runoff quantity and quality. Researchers have utilized various models to manage sewer systems, while others have explored the applicability of rainfall and runoff models to urban areas (Bulti & Abebe 2020). Two models are used to describe

Table 1 | Events selected for calibration and model validation phases

No. of event	Start of rain	End of rain	mm	Use	Code
1	27/09/2016 22:45:00	28/09/2016 14:00:00	21	Calibration	C1
2	12/09/2019 15:30:00	13/09/2019 02:15:00	40.6	Calibration	C2
3	13/12/2018 13:30:00	14/12/2018 19:45:00	48.2	Calibration	C3
4	06/12/2016 20:30:00	07/12/2016 12:45:00	33.6	Calibration	C4
5	23/03/2017 16:15:00	24/03/2017 20:30:00	47.4	Calibration	C5
6	23/11/2015 16:15:00	25/11/2015 00:00:00	36.8	Validation	V1
7	10/01/2017 10:00:00	11/01/2017 14:45:00	47.8	Validation	V2
8	22/03/2016 01:00:00	23/03/2016 09:00:00	31.8	Validation	V3
9	26/11/2015 20:30:00	27/11/2015 10:30:00	26.6	Validation	V4
10	01/10/2018 16:15:00	02/10/2018 06:00:00	18	Validation	V5

these different phenomena: hydrological models to generate a hydrograph at the outlet of each sub-basin and hydraulic models to propagate this hydrograph through the sewer system sections (Brendel *et al.* 2021).

In this study, the coupling of ArcGIS with the MIKE URBAN software developed by the Danish Hydraulic Institute (DHI) is used to model the sewerage network of the Algiers center. This coupling offers a powerful platform for modeling and analyzing urban water systems. The combination of these two software packages enhances geospatial analysis, data integration, and visualization capabilities. The coupling of ArcGIS with MIKE URBAN is implemented in two phases. The first phase involves preparing the data required for the modeling process. ArcGIS is used to create or import geospatial datasets with proper georeferencing. This includes exporting relevant datasets from ArcGIS in a compatible format (Shapefiles) with MIKE URBAN, as well as cleaning and pre-processing the data to ensure compatibility with MIKE URBAN requirements. The second phase occurs after the simulations and focuses on the visualization and analysis of the results. In this phase, the simulation results from MIKE URBAN are imported into ArcGIS for visualization, processing, and analysis. The MIKE URBAN software displays the runoff based on the dimensions of the network inverts, while the runoff processing is carried out according to the Digital Elevation Model (DEM).

MIKE URBAN is powerful hydrological and hydraulic modeling software with a user-friendly interface suitable for sewers of all sizes and types. It is well-suited for analyzing the hydraulic performance of complex looped sewer systems, including overflows, storage basins, and pumping stations. It provides three options for calculating flow depth and velocity: kinematic, diffusive, and dynamic waves (DHI 2017).

The MOUSE software includes all elements constituting the network, such as collectors, junctions (nodes), singularities (storm overflows, drop points, etc.), and lifting stations. These elements play a crucial role in influencing the flow. It is worth noting that network schematization sometimes focuses solely on the main collector to simplify the study. Several bibliographical studies have shown that this simplification does not significantly impact the flow description and system behavior (Kroll *et al.* 2010). Therefore, for this study, the network simplification was conducted based on the main network schematization only. The specification of upstream and downstream boundary conditions is also performed at the system inlet or outlet (outfall) before commencing the two (02) stages of modeling, namely hydrological and hydraulic modeling (as shown in Supplementary material, Figure S1).

3.3.1. Hydrological models using MOUSE

The current study utilizes two primary hydrological models: the Horton model, which is applied when the impervious surface area is less than 30%, and the linear reservoir model, which is applied when the impervious surface area exceeds 30%. In these models, the surface storage depth is represented by YS, and the accumulated depth at time t is denoted as $\gamma(t)$. The production and transfer functions are illustrated in Figure 6.

The hydrological simulations incorporate evaporation, infiltration, and surface storage losses as key mechanisms. These losses are estimated using the equations provided below. However, due to the absence of specific evaporation measurements, this study does not explicitly consider evaporation losses (i.e., they are included in the simulation by incorporating a storage
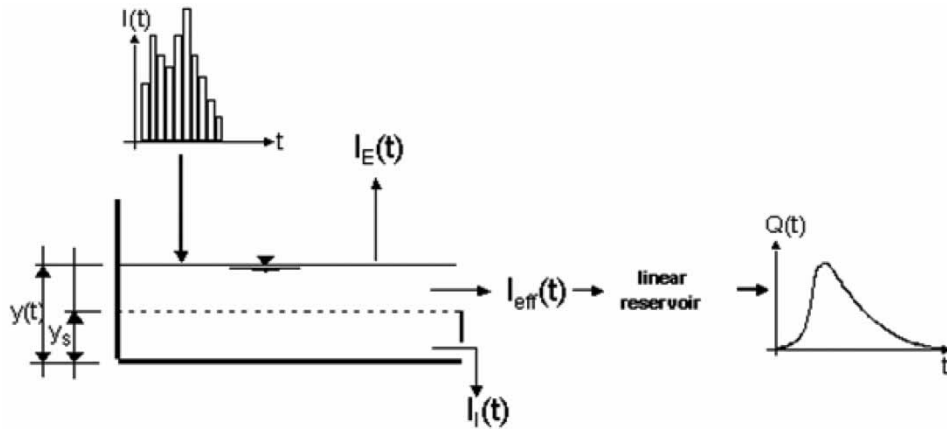
Figure 6 | Processes simulated in the surface runoff Model C (DHI 2017).

loss rate). The effective precipitation, denoted as I_{eff}, represents the remaining precipitation after accounting for these losses. It is generally defined as follows:

$$I_{eff}(t) = I(t) - IE(t) - II(t) - IS(t) \tag{1}$$

where $I(t)$ is the actual precipitation intensity at time t; $IE(t)$ is the evaporation loss at time t; $IS(t)$ is the initial loss (wetting and surface storage) at time t; $II(t)$ is the infiltration loss at time t.

In this context, infiltration ($II(t)$) refers to the water loss that occurs when water seeps into the subsurface storage due to the porosity of the watershed surface. Infiltration is assumed to commence after the surface becomes saturated. The estimation of infiltration loss is determined by applying the following relationships:

$$II(t) = \begin{cases} IH(t), & I(t) - IE(t) \geq IH(t) \\ I(t) - IE(t), & I(t) - IE(t) \, IH(t) \\ 0, & I(t) IE(t) \end{cases} \tag{2}$$

where $II(t)$ is the infiltration loss at time t; $IH(t)$ is the Horton's infiltration at time t (see the following).

The model utilized the renowned Horton's equation to compute the capacity for permeation loss. By default, the original form of Horton's equation was employed:

$$IH(t) = II_{min}(t) + (II_{max} - II_{min}) . e^{-ka\,t} \tag{3}$$

where $IH(t)$ is the infiltration loss calculated according to Horton; II_{max} is the maximum infiltration capacity (after a long dry period); II_{min} is the minimum infiltration capacity (at full saturation); t is the time since the start of the storm; ka is the time factor (characteristic soil parameter) for wetting conditions.

The cumulative infiltration, $I_{cum}(t)$, at time t corresponds to the area under the Horton curve. It represents the accumulated amount of infiltrated water over time. In this study, the infiltrated water is estimated by integrating the Horton infiltration equation mentioned earlier:

$$I_{cum}(t) = \int_0^t II(t)dt \tag{4}$$

The transfer function utilized in this study is based on the linear reservoir model, which is a simple conceptual model to apply. It only requires one parameter, referred to as 'k,' which represents a reservoir that linearly delays the arrival of rainfall.

The coefficient 'k' is known as the lag time and represents the storage time in the reservoir. It indicates the temporal shift between the barycenter of the net rainfall hyetograph (rainfall distribution over time) and the hydrograph (flow rate variation

over time) at the basin outlet. The linear reservoir model assumes that the storage volume is solely a linear function of the outflow, unlike the nonlinear reservoir model where it depends on both the inflow and outflow in a nonlinear manner. Additionally, the production and transfer functions are assumed to be independent of the initial soil water status. The hydraulic simulation and details of the linear reservoir model are well-described (Chocat 1997).

In MOUSE, the linear reservoir model is represented by the C model. This runoff model, referred to as Model C, is based on the volume continuity and linear reservoir equations. There are two versions of the C model implemented: C1 used in the Netherlands, and C2 used in France. The difference between these two models, C1 and C2, lies in the estimation equation for the constant C.

For Model C1, the constant C is estimated using the following equation:

$$C = A.T_c \tag{5}$$

The estimation of Model C2 involves calculating the constant C as the reciprocal of K, which can be expressed as:

$$C = \frac{A}{T_L} \tag{6}$$

where A is the total catchment surface area; TL is the catchment lag time.

Moreover, the model offers an empirical formula to calculate the reciprocal value of the linear reservoir constant K as:

$$K = 0.3175. \, A^{\wedge}(-0.0076). \, IMP^{\wedge}(-0.512).L^{\wedge}0.608.S^{\wedge}(-0.401) \tag{7}$$

where A is the total catchment surface area (ha); IMP is the impervious part of the catchment (0–1); S is the catchment slope (%); L is the catchment length (m).

Our project is based on selecting the French Model C2, primarily due to the involvement of French experts in the management of the sewerage network in Algiers. The calculation of runoff volume depends on factors such as initial losses, the size of the contributing area, and losses through infiltration. The initial step involves determining the effective rainfall intensity. Additionally, the effective rainfall amount refers to the portion of rainfall that directly contributes to surface runoff:

$$Q(t) = C.y_R(t) \tag{8}$$

$$I_{eff}(t).A \ - Q(t)C = A \frac{dY_R}{dt} \tag{9}$$

where C is the linear reservoir constant; $y_R(t)$ is the runoff depth at time t; I_{eff} is the effective precipitation; A is the contributing catchment surface area; dt is the time step; dY_R is the change in runoff depth.

3.3.2. Hydraulic models using MOUSE

Hydrological simulation plays a crucial role in predicting flooding events within a specific return period (Hingray 2014) and assessing the associated damages by identifying vulnerable areas. It serves as the fundamental element for conducting hydrological studies.

The 'MIKE URBAN' software offers three options for approximating flow: the dynamic wave approach, diffusive wave approach, and kinematic wave approach. The diffusive and kinematic wave approximations are simplified versions of the complete dynamic descriptions. Hence, the dynamic mode is preferred as it encompasses all scenarios. Dynamic routing utilizes the mechanics equations of the Saint-Venant model, which are derived from the Navier-Stokes equations for flow conditions. It ensures the conservation of mass (continuity equation) and the conservation of momentum (dynamic equation). The general form of these equations is as follows:

Continuity equation for mass conservation:

$$\frac{\partial Q}{\partial x} + \frac{\partial A}{\partial t} = 0 \tag{10}$$

Equation for the conservation of momentum:

$$\frac{\partial Q}{\partial t} + \frac{\partial(\alpha(Q2/A))}{\partial x} + g\frac{\partial y}{\partial x} + gAI_f = gAI_0 \tag{11}$$

where Q is the discharge [m^{3}s^{-1}]; A is the flow area, [m^2]; y is the flow depth, [m]; g is the acceleration of gravity, ms^{-2}; x is the distance in the flow direction, [m]; t is the time, [s]; I_0 is the bottom slope; I_f is the friction slope.

The pressure losses resulting from resistance in free surface flow connections are accounted for using Manning's explicit formula. The equation presented below estimates these losses:

$$I_f = \frac{Q|Q|}{M^2 A^2 R^{4/3}} \tag{12}$$

The Manning number, denoted as M (or $n = 1/M$), represents the conduit's wall roughness. In the equations, A refers to the area, and R represents the hydraulic radius. The use of $Q|Q|$ instead of Q^2 simplifies computations, particularly when dealing with reverse flow scenarios. These equations are applicable to free surface flows. However, they can be generalized to include flows under pressure by incorporating a fictitious space within the pipe. The Preissman gap, implemented in the MIKE URBAN software, is utilized for loaded flows with an unlimited threshold (Chow *et al.* 1988).

3.3.3. Calibration and validation of the model

To effectively achieve the primary objective of mitigating flood risks by delineating flood zones using decision support tools, decision-makers should follow the following steps. The initial phase involves collecting comprehensive and up-to-date data on various flood risk factors, including terrain characteristics, hydrology, rainfall patterns, soil conditions, historical flood records, infrastructure, and land use information. This data collection aims to gain a thorough understanding of the area's vulnerability.

The second phase focuses on conducting a flood risk assessment using the decision support tool, specifically the 'MIKE URBAN' software, which incorporates hydrological and hydraulic models to simulate water behaviour during flood events. The collected data are analyzed to identify high-risk areas and evaluate the potential extent, depth, and impact of flooding.

The third phase entails utilizing decision support tools such as Geographic Information Systems (GIS) to integrate and analyse spatial data for the delimitation of flood zones. GIS enables decision-makers to visually overlay different layers of information, facilitating the identification of high-risk areas and the delineation of flood zones.

These three processes are elaborated in Figure 7, illustrating the methodology employed to develop a reliable decision support tool. Among these processes, calibration holds significant importance and is a critical phase in our methodology's sequence.

In recent decades, the literature has extensively discussed the calibration of flood models, highlighting various criticisms that limit the acceptance of calibrated flood models (Brendel *et al.* 2021). These limitations arise from unreliable measurements used in the calibration phase, particularly in developing countries, and the unavailability of other required parameters (Nkwunonwo *et al.* 2020).

The calibration and validation phases are crucial for the utilization of developed models as they determine the predictive capability of the models. To calibrate the model parameters, we chose an event simulation approach since rain events may not fully capture all the rainfall responsible for critical network overflows (Chocat & Cabane 1999). Manual calibration through trial and error was employed; adjusting the parameters until the observed results closely matched the simulated results (Brendel *et al.* 2021). The dataset was divided into two parts, allocating 50% for calibration and 50% for validation. This approach ensured the development of a robust model capable of delivering accurate results even under extremely heavy rain conditions. The selection of events for calibration based on peak and duration played a significant role in reducing parameter uncertainty.

Successful modeling also relies on effective model calibration and validation, which ensures that the calculated results reasonably correspond to observed flow data. Calibration and validation are crucial engineering aspects of the modeling process and require careful attention (Moriasi *et al.* 2015).
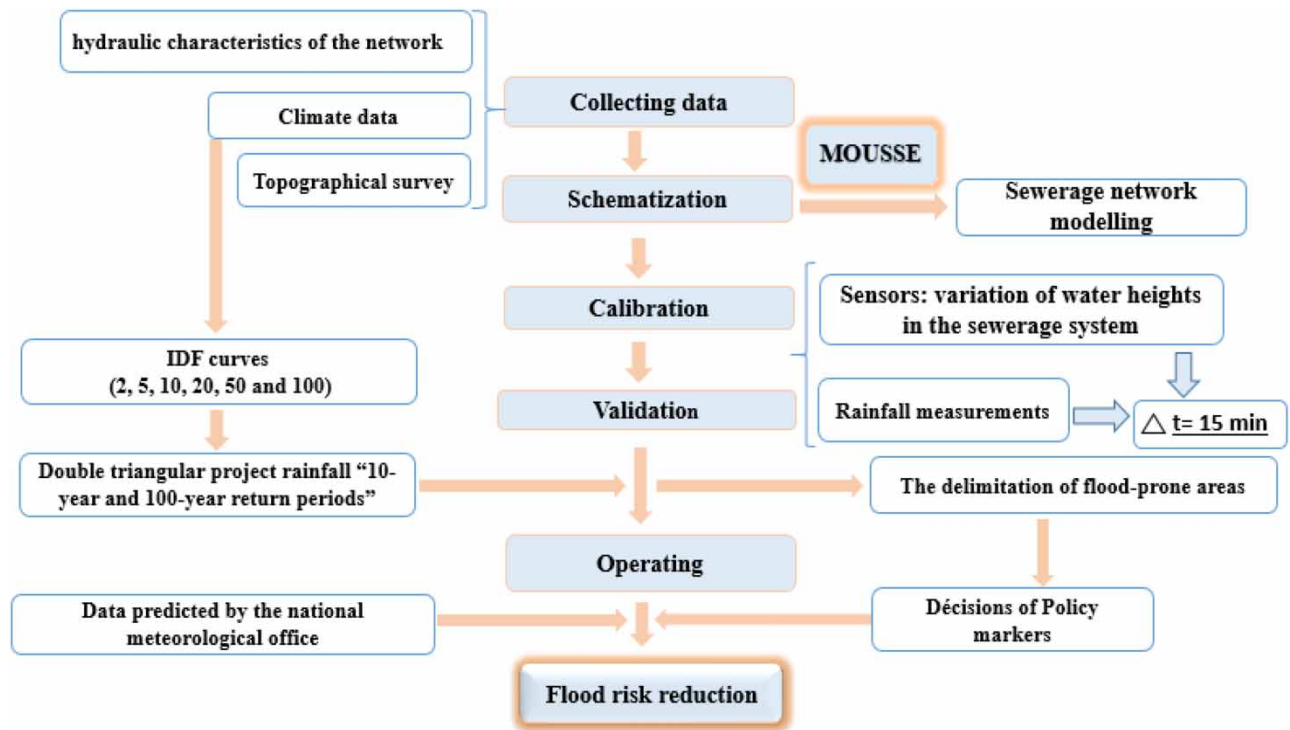
Figure 7 | Illustration of our methodology.

In this research, manual calibration through trial and error was performed to align the measured parameters with the model's predicted values, aiming for the closest possible fit. This was followed by the validation phase, which aimed to test assumptions independent of those used in calibration to verify the model's performance and ensure its realism. The events selected for both calibration and validation stages encompassed medium to high rainfall intensities with durations ranging from 30 min to 24 h.

4. RESULTS AND DISCUSSION

The increasing frequency of extreme rainfall events due to climate change presents a significant challenge to urban resilience, necessitating changes in the planning, speed, and redundancy of flood-affected communities (Xu *et al.* 2023). This study proposes a modernized approach to flood management by implementing sensors within the sewage network. Among all the regions in Algeria, Algiers is the only area equipped with hydraulic sensors. The installation of these sensors aims to transfer signals and information to network managers. The crucial information for them includes exceeding specific water levels or predefined thresholds that trigger alerts during exceptional events. In other words, these warning signals serve to protect people from floods during disasters.

Unfortunately, many of the installed sensors were lost during exceptional floods. For the remaining sensors, the lack of understanding among managers regarding the value of the recorded data series poses a challenge. It is essential to utilize this data and employ modeling techniques to predict flow patterns before a flood occurs, rather than relying solely on real-time measurements during a flood. Failure to address this concern could make risk management significantly more challenging in terms of protecting lives and property from this major threat.

The figures presented below illustrate the outcomes of our methodology (refer to Figure 7). For each event used in the analysis (as shown in Table 1), we have included two graphical representations. The first graph depicts the variation in observed and simulated water levels over time for both the calibration and validation phases. The second graph compares the simulated results with the observed measurements (refer to Figures 8–22). Overall, the results demonstrate a good fit between the water levels predicted by our model and those measured by the AN1 and AN3 sensors (refer to Figure 1(d)).
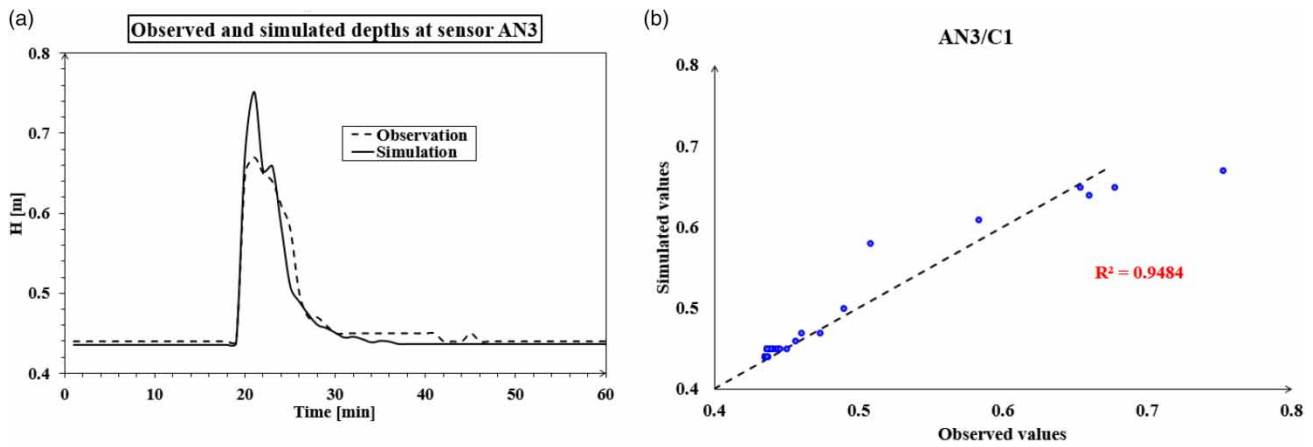
(a)

Observed and simulated depths at sensor AN3

(b)

AN3/C1

R² = 0.9484

Figure 8 | Observed and simulated depths at Sensor AN1 during the calibration phase, which corresponds to rainfall Event 1 (see Table 1).
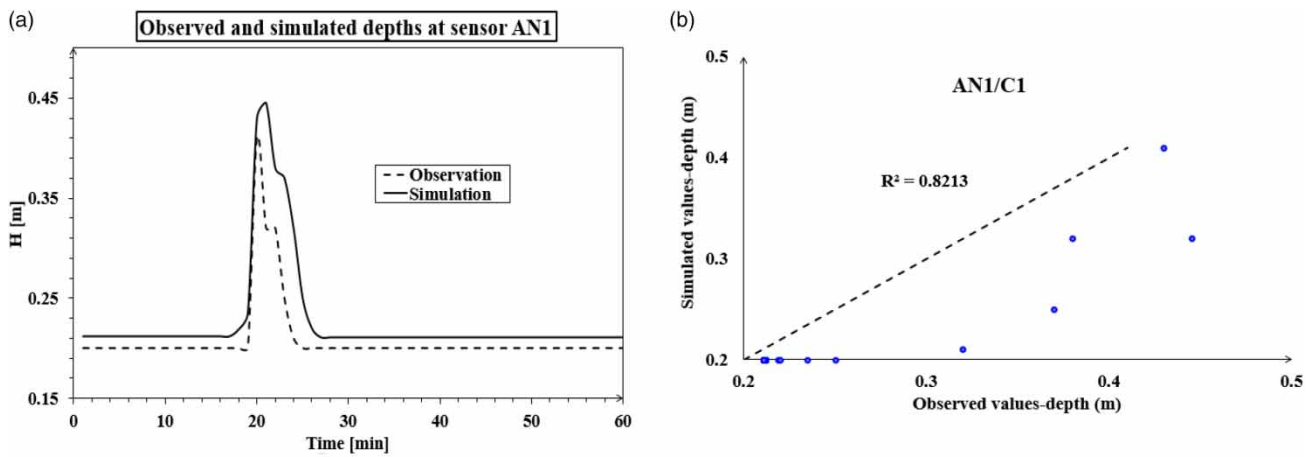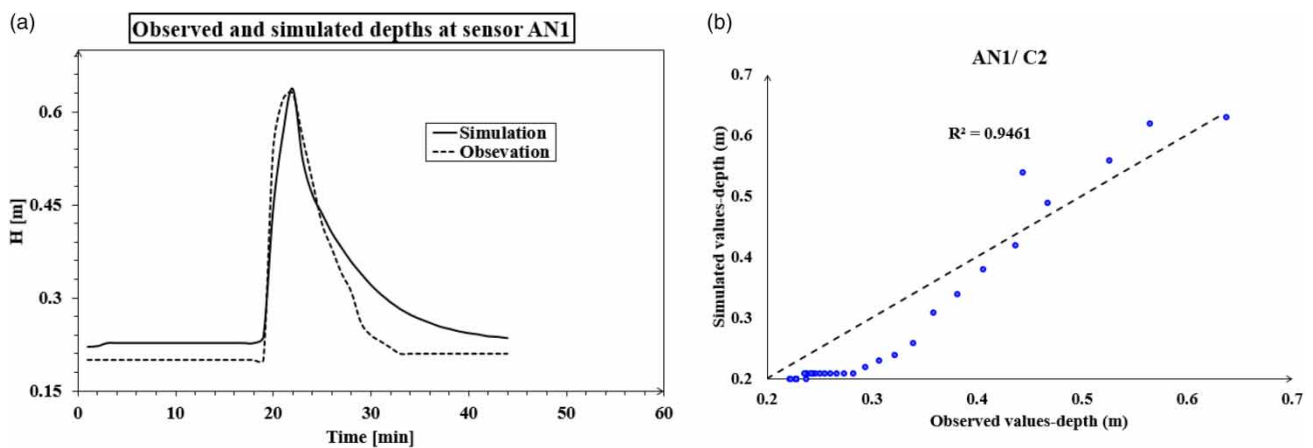
(a)

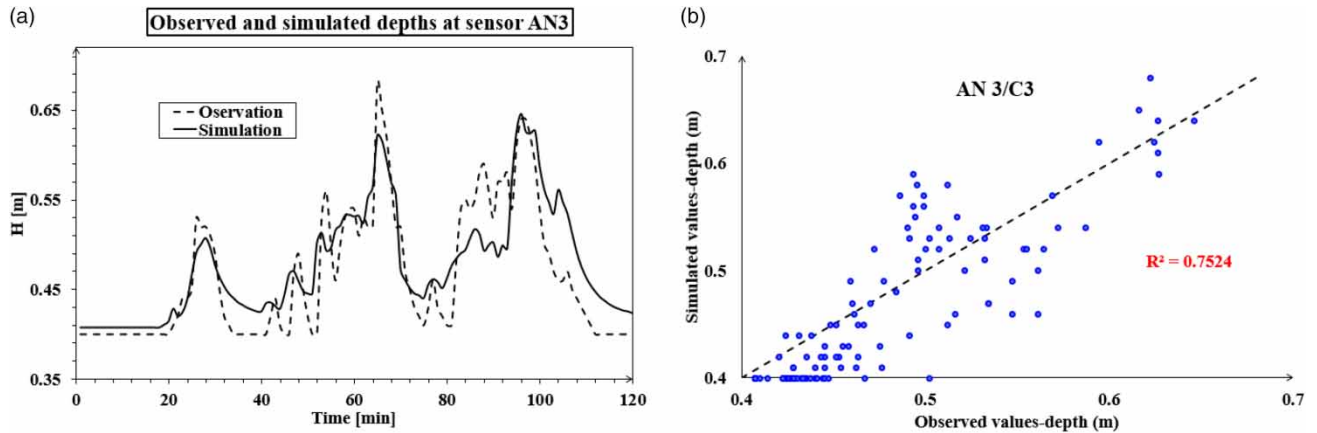**Observed and simulated depths at sensor AN1**

(b)

AN1/C1

R² = 0.8213

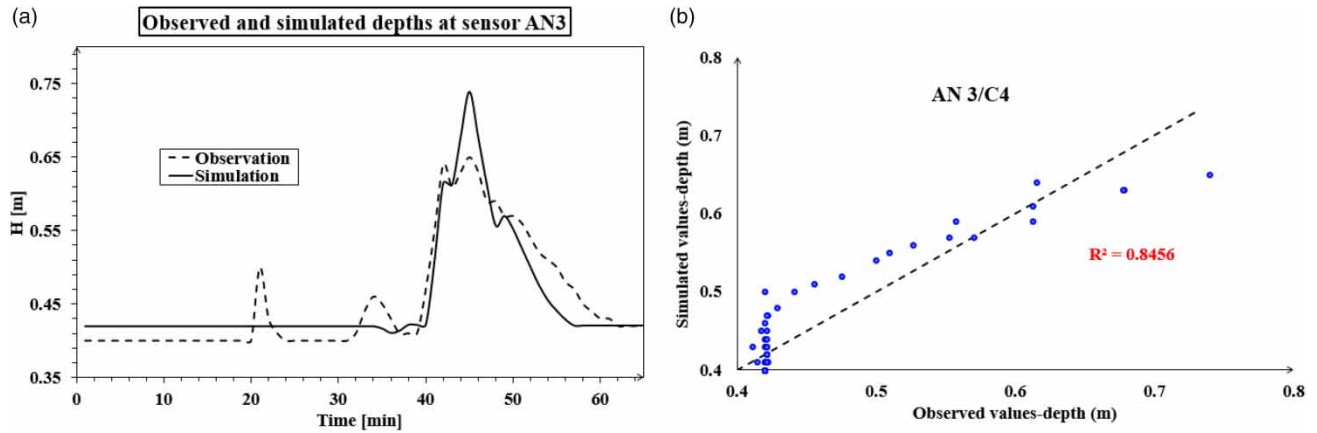**Figure 9** | Observed and simulated depths at Sensor AN3 during the calibration phase, which corresponds to rainfall Event 1 (see Table 1).

(a)

Observed and simulated depths at sensor AN1

(b)

AN1/ C2

R² = 0.9461

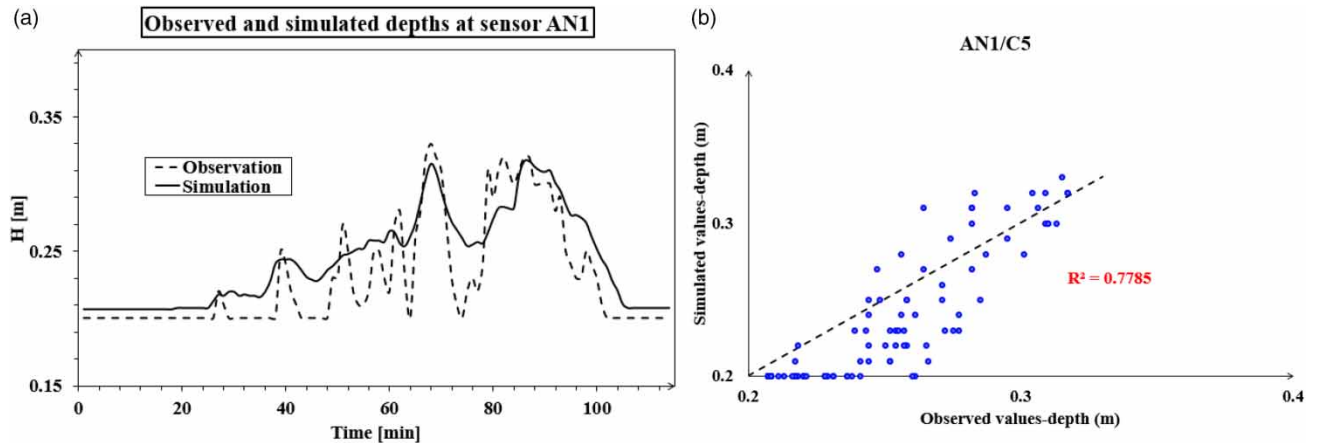**Figure 10** | Observed and simulated depths at Sensor AN1 during the calibration phase, which corresponds to rainfall Event 2 (see Table 1).

(a)

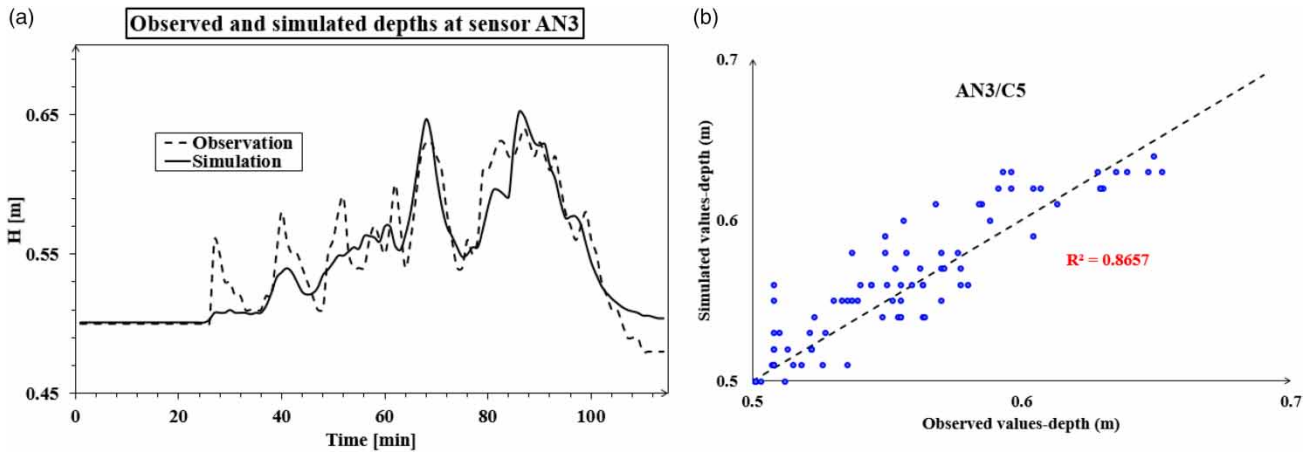**Observed and simulated depths at sensor AN3**

(b)

AN 3/C3

R² = 0.7524

Figure 11 | Observed and simulated depths at Sensor AN3 during the calibration phase, which corresponds to rainfall Event 3 (see Table 1).

(a)

Observed and simulated depths at sensor AN3

(b)

AN 3/C4

R² = 0.8456

Figure 12 | Observed and simulated depths at Sensor AN3 during the calibration phase, which corresponds to rainfall Event 4 (see Table 1).

(a)

Observed and simulated depths at sensor AN1

(b)

AN1/C5

R² = 0.7785

Figure 13 | Observed and simulated depths at Sensor AN1 during the calibration phase, which corresponds to rainfall Event 5 (see Table 1).

Figure 14 | Observed and simulated depths at Sensor AN3 during the calibration phase, which corresponds to rainfall Event 5 (see Table 1).
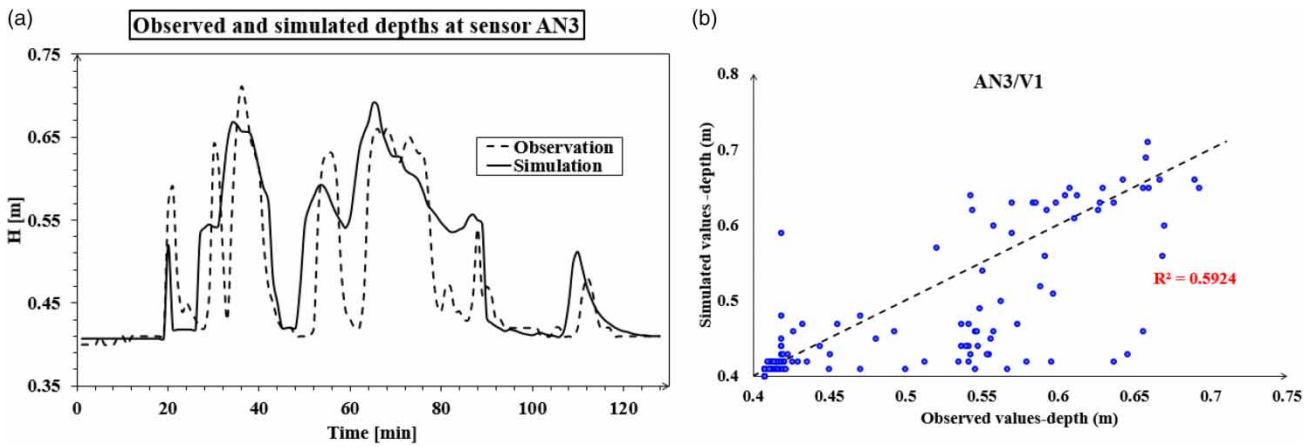

Figure 15 | Observed and simulated depths at Sensor AN3 during the validation phase, which corresponds to rainfall Event 6 (see Table 1).
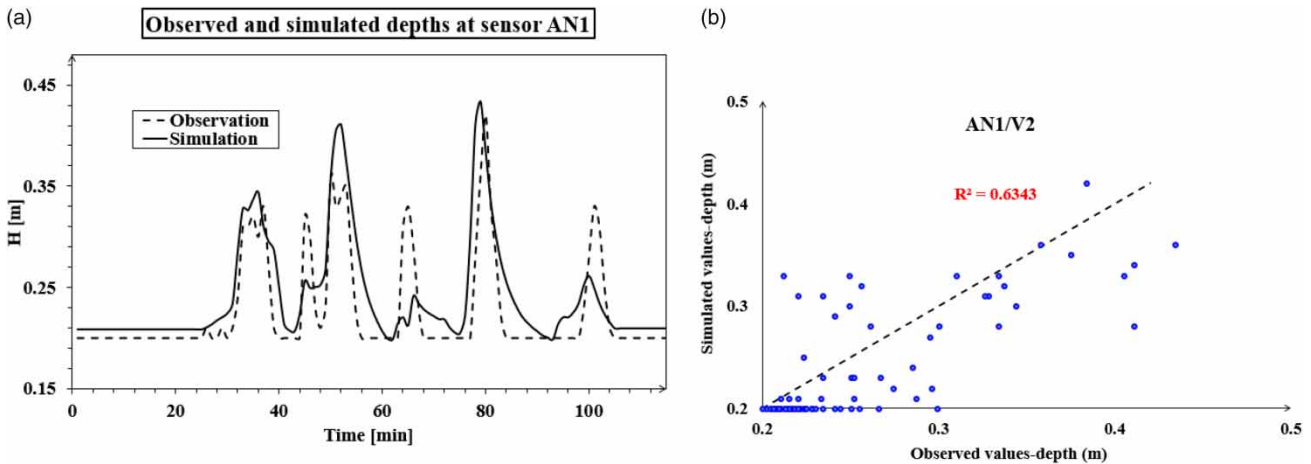

Figure 16 | Observed and simulated depths at Sensor AN1 during the validation phase, corresponding to rainfall Event 7 (see Table 1).
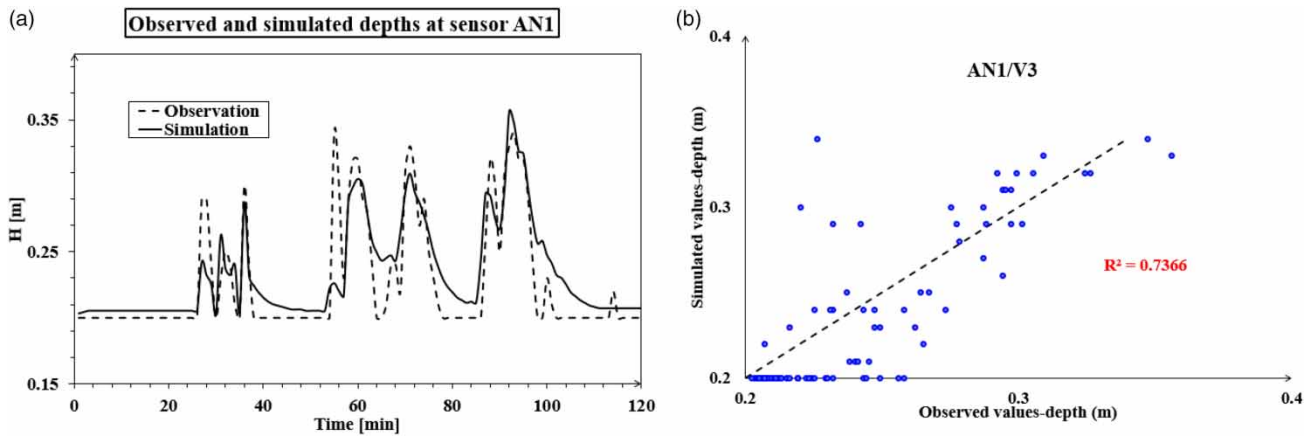
Figure 17 | Observed and simulated depths at Sensor AN1 during the validation phase, corresponding to rainfall Event 8 (see Table 1).

Figure 18 | Observed and simulated depths at Sensor AN3 during the validation phase, corresponding to rainfall Event 8 (see Table 1).

Figure 19 | Observed and simulated depths at Sensor AN1 during the validation phase, corresponding to rainfall Event 9 (see Table 1).
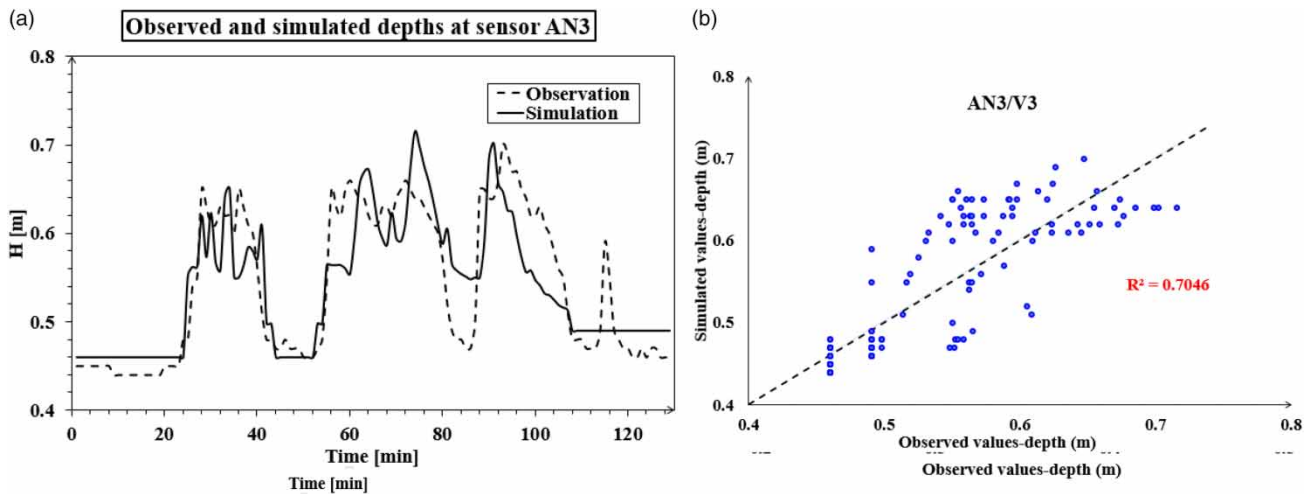
Figure 20 | Observed and simulated depths at Sensor AN3 during the validation phase, corresponding to rainfall Event 9 (see Table 1).

Figure 21 | Observed and simulated depths at Sensor AN1 during the validation phase, corresponding to rainfall Event 10 (see Table 1).
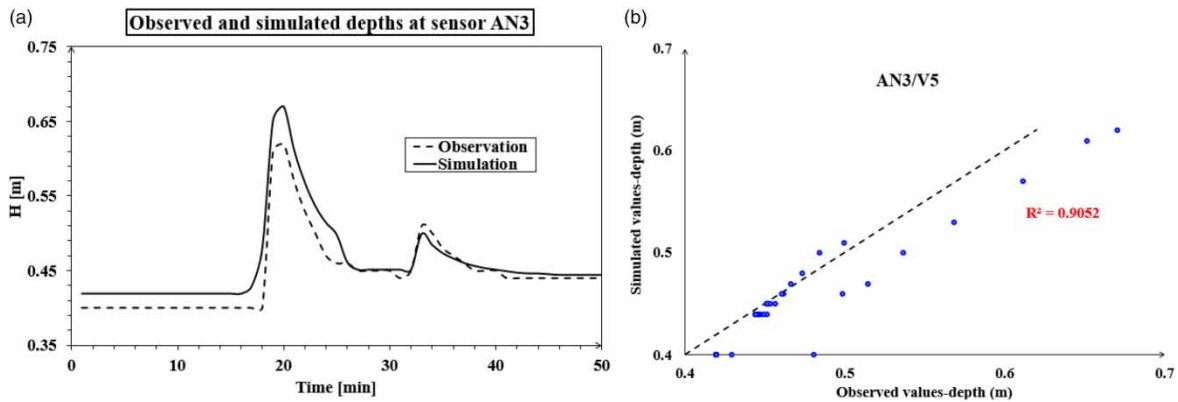
Figure 22 | Observed and simulated depths at Sensor AN3 during the validation phase, corresponding to rainfall Event 10 (see Table 1).
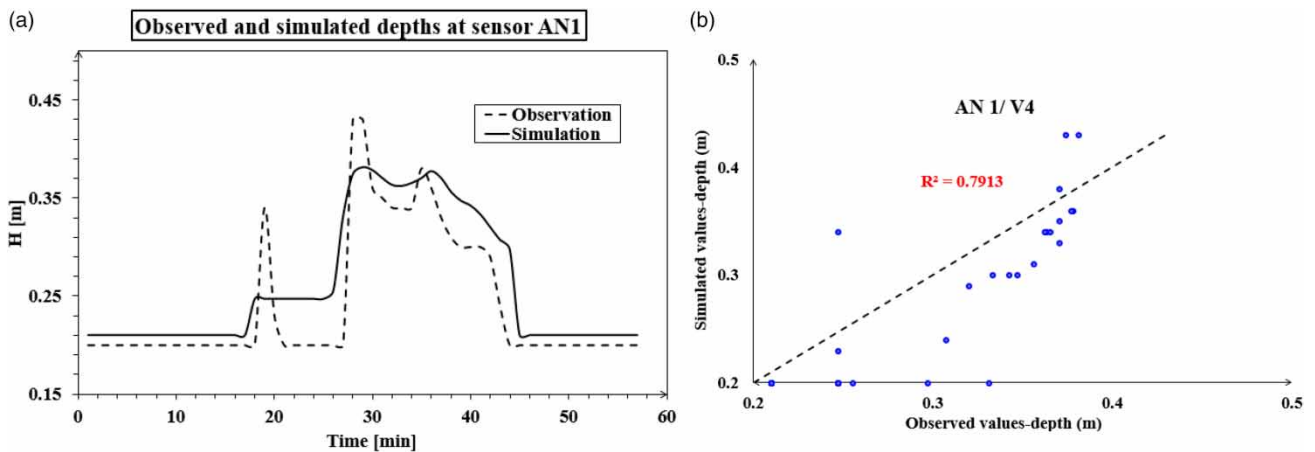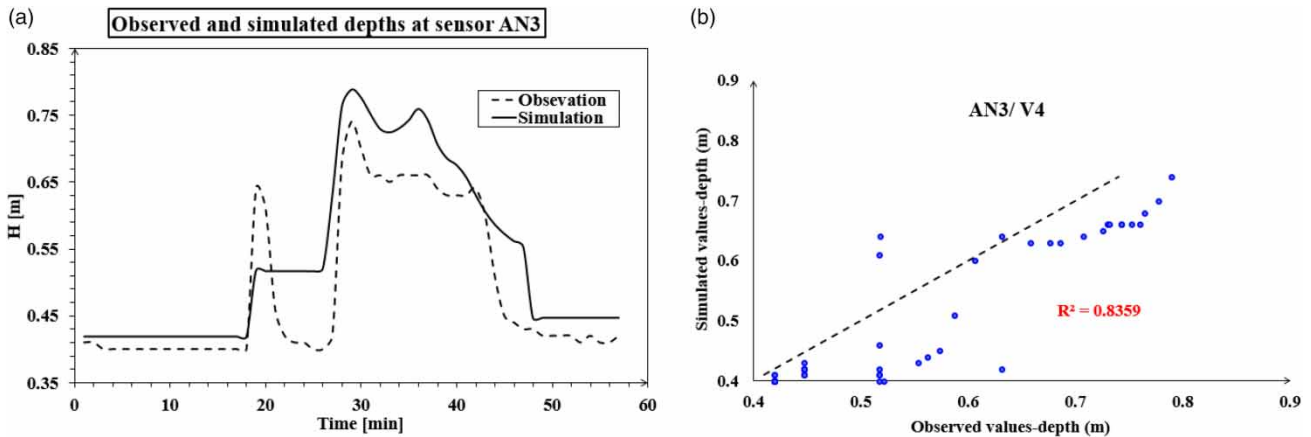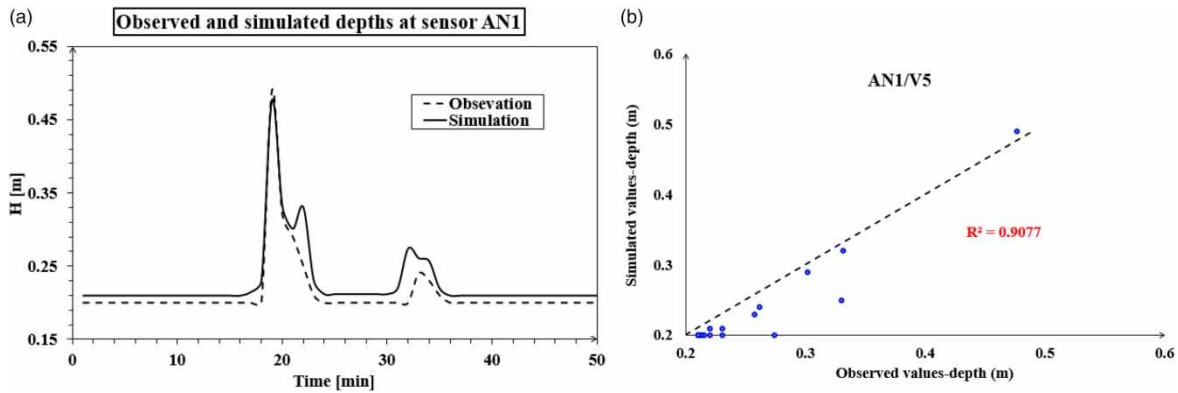
The evaluation of model performance is crucial in various fields, including hydrology, climate modeling, and environmental sciences, and it often relies on performance criteria. It is important to note that the choice of performance criteria may vary depending on the specific context and objectives of the modeling study (Moriasi *et al.* 2015).

Many researchers in flood modeling acknowledge the presence of errors and uncertainties in developed flood models (Moriasi *et al.* 2015; Nkwunonwo *et al.* 2020; Tamiru & Wagari 2021). Therefore, assessing the performance of a hydrological or water quality model during the calibration and validation phases is a critical step as it provides valuable insights for selecting appropriate parameters and understanding the phenomenon at hand. In our study, we employed several performance criteria, including NSE, R^2, RMSE, and PBIAS, to validate the developed model.

Previous studies have demonstrated that as the impermeability coefficient increases, the infiltration capacity decreases, resulting in higher runoff and elevated peak flow rates (Nkwunonwo *et al.* 2020). Considering this relationship, the calibration process focused on the impermeability coefficient, which represents the portion of the active surface contributing to runoff, as well as the reduction coefficient, which signifies the proportion of runoff effectively entering the network, accounting for initial losses and lag time. Subsequently, the model was calibrated and validated using available *in situ* measurements to ensure its robustness in replicating the rain-flow transformation in an urban environment.

The following table summarizes the various criteria used to evaluate the performance of our model:

Based on the summary table of performance criteria (Table 2), the findings of this article can be summarized as follows: Calibration:

- Nash–Sutcliffe Efficiency (NSE) > 0.67: The NSE value exceeding 0.67 indicates a good fit between the simulated and observed data during the calibration period. It signifies that the model adequately captures the variability of the observed data.
- R^2 > 0.75: With an R^2 value greater than 0.75, the model demonstrates a substantial correlation with the observed data, explaining a significant portion of its variation.
- RMSE < 6%: The RMSE, which measures the average difference between the simulated and observed data, is less than 6%. This indicates a relatively low level of inaccuracy between the model and the observed data.
- PBIAS ≤ ±11%: The PBIAS, evaluating the model's bias in predicting observed values, falls within ± 11% during the calibration period. This indicates an acceptable level of bias in the model's predictions.

Validation:

- NSE > 0.50: Similar to the calibration phase, an NSE value greater than 0.50 signifies a good fit between the model and observed data during the validation period.
- R^2 > 063: An R^2 score higher than 0.63 indicates a reasonably strong correlation between the model and observed data throughout the validation phase.
- RMSE < 7%: The RMSE value is less than 7%, implying that the model's predictions are relatively accurate compared to the observed data during the validation period.
- PBIAS ≤ ±10%: The PBIAS value, which measures the model's bias in predictions, is within ± 10%, indicating an acceptable level of bias in the model's performance during the validation period.

Based on the validation results obtained with the selected events, the criteria indicate a good and satisfactory fit for the pilot area. The observed and simulated curves for the two sensors generally exhibit the same pattern. Considering these

Table 2 | Performance evaluation criteria

		R^2		RMSE [%]		NSE		PBIAS [%]	
		AN 1	AN 3	AN 1	AN 3	AN 1	AN 3	AN 1	AN 3
Calibration	C1	0.82	0.95	3.04	1.63	0.68	0.92	−8.98	1.04
	C2	0.95	–	5.47	–	0.79	–	−10.83	–
	C3	–	0.75	–	3.78	–	0.73	–	−2.38
	C4	–	0.85	–	2.97	–	0.84	–	−0.22
	C5	0.78	0.87	2.32	1.71	0.67	0.86	−5.76	0.41
Validation	V1	–	0.59	–	6.46	–	0.52	–	−4.42
	V2	0.63	–	3.53	–	0.50	–	−5.79	–
	V3	0.74	0.70	2.23	4.53	0.71	0.70	−2.97	0.44
	V4	0.79	0.84	3.68	6.90	0.70	0.63	−8.02	−9.45
	V5	0.91	0.91	1.90	2.16	0.81	0.80	−6.41	−3.08

representations and the validation results of NSE, R^2, RMSE, and PBIAS, it can be concluded that the model developed for this sub-watershed is reliable for practical use.

These performance criteria provide a comprehensive assessment of the model's accuracy and reliability in capturing observed data. Meeting or exceeding these criteria indicates that the model performs well in both calibration and validation, demonstrating its potential for credible flood risk predictions and simulations.

After the model validation process, two simulations were conducted on the entire sewerage network of the central part of Algiers, utilizing the projected rainfall data for the 10-year and 100-year return periods. The simulation results for the 10-year return period are presented in Figure 23, which is of particular interest for evaluating the capacity of the urban network as required by the Algerian water code. On the other hand, the results of the simulation with the 100-year rainfall are crucial for estimating potential overflows outside the network during exceptional flood events, as depicted in Figure 24. Additionally, synoptic diagrams (Figures A3–A10) are employed to provide detailed visual representations of the various flow characteristics observed in the calibrated pilot example.

The main sewerage network under study is characterized by a diameter of 1 m and varying slopes, including low, medium, and very high slopes (refer to Supplementary material, Figure S2). For a 100-year return period, approximately 90% of the studied section exhibits flow velocities exceeding 4 m/s (see Supplementary material, Figure S8). In contrast, for the 10-year return period, only 15% of the network experiences flow velocities exceeding 4 m/s (see Supplementary material, Figure S7). Notably, along a linear stretch constituting 20% of the total, the flow velocities result in a flow rate exceeding 3 m^3/s for the 100-year return period, as depicted in Supplementary material, Figures S9 and S10.

Supplementary material (Figures A3 and A4) indicates that flow within the network accounts for approximately 30% during the 10-year return period and nearly 50% during the 100-year return period. Consequently, the assurance of free surface flow is not guaranteed. In terms of overflows occurring outside the sewerage network through storm overflows, 10% of the storm overflows are characterized by overflow heights of less than 0.3 m (see Supplementary material, Figure S5). However, for the 100-year return period, 30% of the spillways experience water heights exceeding 0.5 m at spillway No. 6 (refer to Supplementary material, Figure S6). Thus, it is evident that the main network in the study area is incapable of effectively handling rainfall corresponding to either a 10-year return period or a 100-year return period flood event. Through our comprehensive analysis, we have identified 300 overflow points in the Algiers sewerage network during simulations conducted with a 10-year rainfall event, and 400 points during simulations conducted with a 100-year rainfall event.
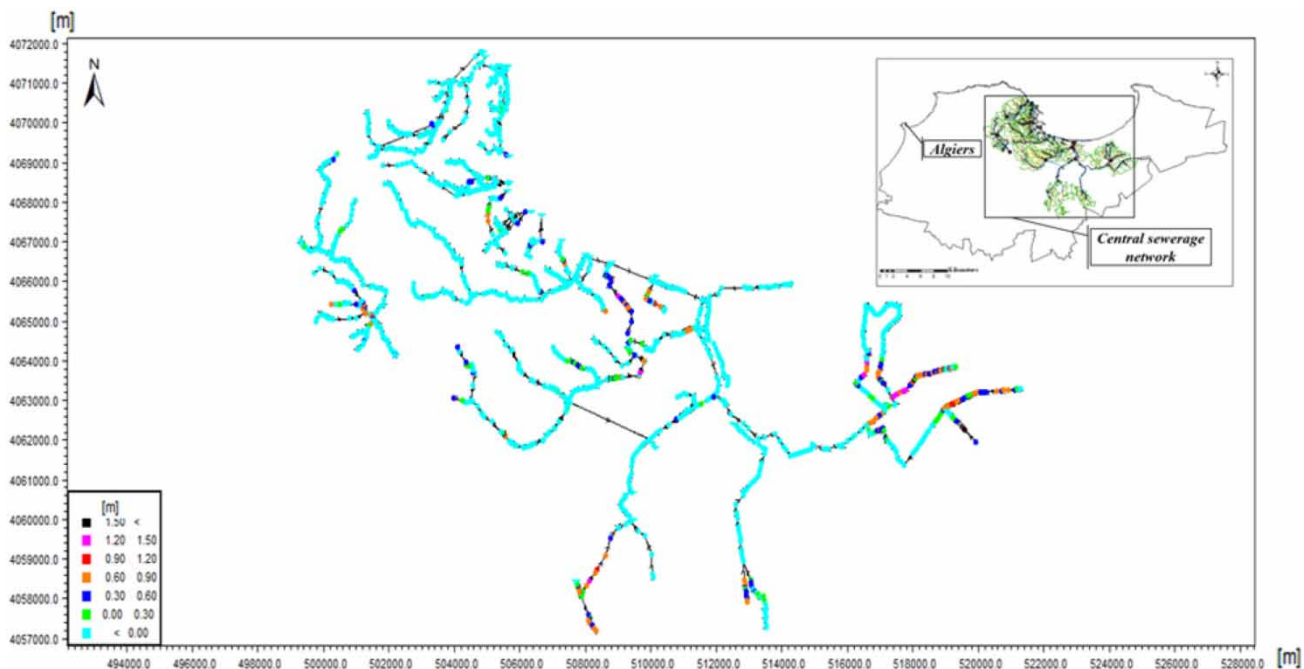

Figure 23 | Overflow point simulation with a projected rainfall that corresponds to the 10-year return period.
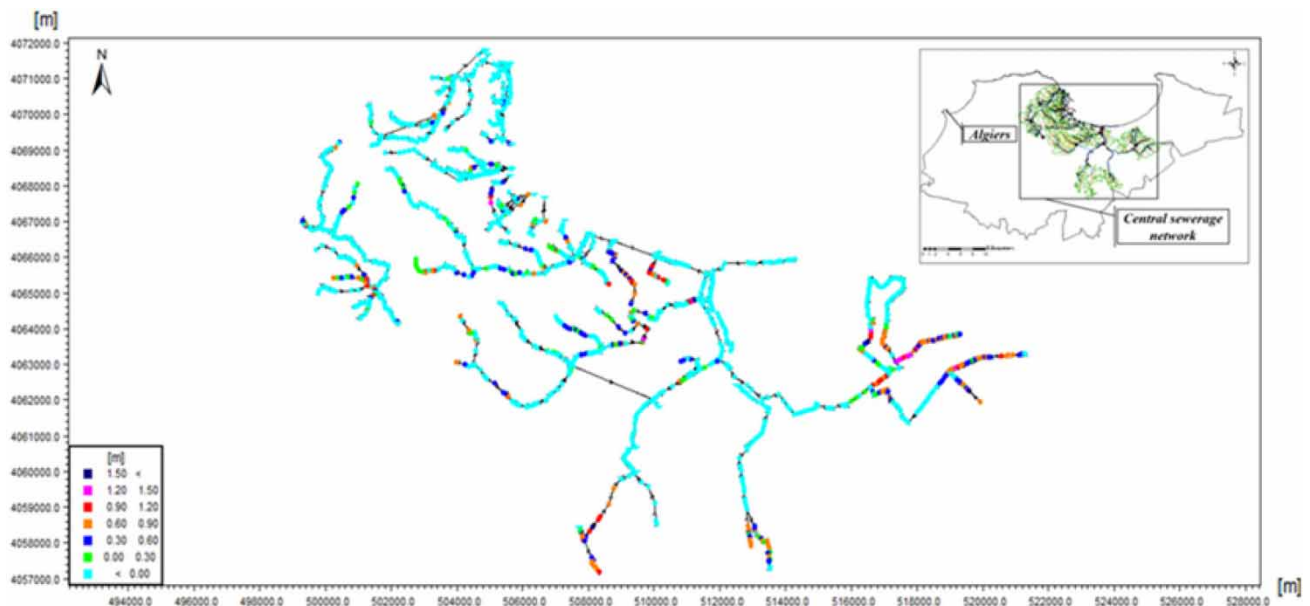
Figure 24 | Overflow point simulation with a projected rainfall that corresponds to the 100-year return period.

Table 3 | Summary of the simulation results conducted on all central sewerage networks of Algiers

Flooded water level Range	Number of flooding points		Relative to the total number [%]		Change in the number of flood points [%] Comparing the 100-year/ the 10-year flood
	10 year	100 year	10 year	100 year	
0–0.3	93	118	28.79	24.95	26.88
0.3–0.6	117	166	36.22	35.10	41.88
0.6–0.9	91	139	28.17	29.39	52.75
0.9–1.2	8	29	2.48	6.13	262.50
1.2–1.5	11	14	3.41	2.96	27.27
>1.5	3	7	0.93	1.48	133.33
Total number of flood points	**323**	**473**	**100**	**100**	**46.44**

The ratio of overflow points corresponding to the 100-year rainfall compared to the 10-year rainfall exhibits an increase of 46% (refer to Table 3). For example, in the main network of Algiers, there are 117 overflow points characterized by water heights ranging from 0.3 to 0.6 m during a 10-year return period rainfall event. Conversely, for the same duration, 166 overflow points are identified for rainfall events with a 100-year return period (see Figure 25). Detailed results for other flooded water levels are presented in Figure 25. Further comparisons between the simulation results of the two rainfall events can be found in Table 3 and Figure 4.

5. CONCLUSIONS

In this study, the drainage network of Algiers, Algeria, was modeled and the hydraulic performance of the system was evaluated. The research utilized real-time sub-hourly observations from the sewage network to enhance flood control through numerical modeling. The development of a valid and effective model for urban flood control will be beneficial to decision-makers and urban planners.

During model validation, performance metrics such as NSE, R^2, RMSE, and PBIAS were used. The results showed that NSE was greater than 0.50, R^2 was approximately 0.63, RMSE was 7%, and PBIAS was 10%, indicating the model's
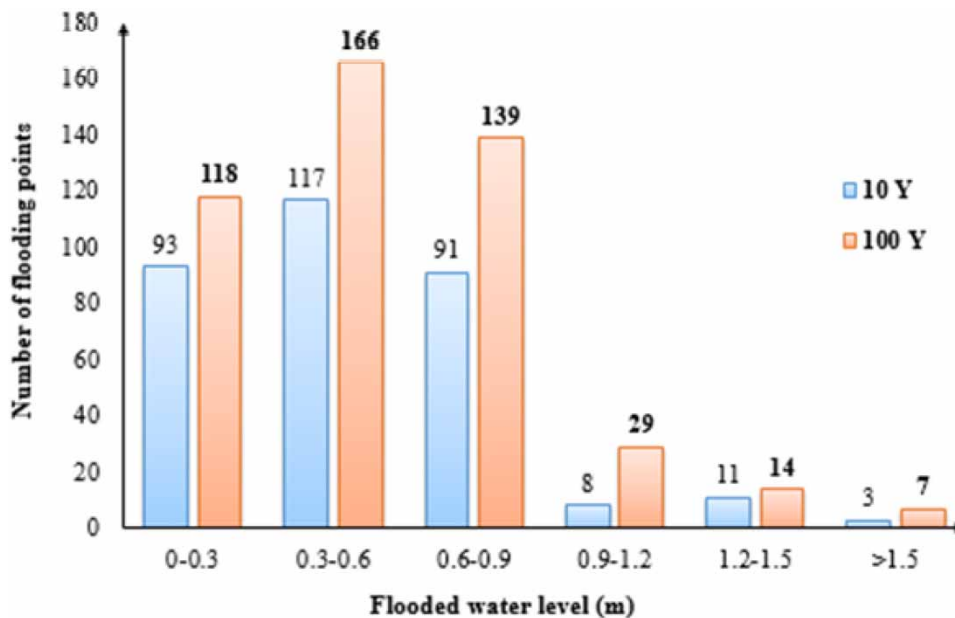
Figure 25 | The relationship between flooded water levels and the corresponding variation in flooding points.

reliability. By utilizing preferred flow axes, the major overflow points were identified, and water levels for different flood scenarios (annual, 10-year return period, and 100-year return period) were calculated.

The mapping of major flood zones in Algiers and the identification of high overflow areas resulting from exceptional rainfall (exceeding 0.5 m) provide valuable information for disaster mitigation. The model's performance allows decision-makers and managers to predict flow behaviour in the sewer system and estimate overflow rates based on precipitation forecasts.

However, there are certain limitations to this study. It focused solely on urban catchments and modeled only main storm sewer pipes, neglecting auxiliary storm sewer conduits that could have improved the model's estimated hydrological responses. Additionally, model validation relied on extreme event simulations rather than continuous simulations, and groundwater-related processes were not simulated. The number of sensors placed on the sewage network was limited, which could have impacted the calculation efficiency and introduced uncertainties in the model's results.

To address these limitations, it is recommended to consider additional sensors in the pluvial drainage network to decrease uncertainties and enhance the model's reliability. Moreover, incorporating auxiliary storm sewer conduits and simulating groundwater-related processes would further improve the accuracy of the model. Each urban sub-basin may exhibit different characteristics, such as soil use, drainage systems, and pluviometry, which should be taken into account to obtain reliable results.

DATA AVAILABILITY STATEMENT

All relevant data are included in the paper or its Supplementary Information.

CONFLICT OF INTEREST

The authors declare there is no conflict.

REFERENCES

Abdelkarim, A., Gaber, A. F. D., Youssef, A. M. & Pradhan, B. 2019 Flood hazard assessment of the urban area of Tabuk City, Kingdom of Saudi Arabia by integrating spatial-based hydrologic and hydrodynamic modeling. *Sensors (Basel)* **19**, 1024. https://doi.org/10.3390/s19051024.

Abdrabo, K. I., Kantoush, S. A., Saber, M., Sumi, T., Habiba, O. M., Elleithy, D. & Elboshy, B. 2020 Integrated methodology for urban flood risk mapping at the microscale in ungauged regions: A case study of Hurghada, Egypt. *Remote Sensing* **12** (21), 3548. https://doi.org/10.3390/rs12213548.

Abdrabo, K. I., Hamed, H., Fouad, K. A., Shehata, M., Kantoush, S. A., Sumi, T., Elboshy, B. & Osman, T. A. 2021 Methodological approach towards sustainable urban densification for urban sprawl control at the microscale: Case study of Tanta, Egypt. *Sustainability* **13** (10), 5360.

Abdrabo, K. I., Kantosh, S. A., Saber, M., Sumi, T., Elleithy, D., Habiba, O. M. & Alboshy, B. 2022a The role of urban planning and landscape tools concerning flash flood risk reduction within arid and semiarid regions. In: *Wadi Flash Floods*. Springer, Singapore, pp. 283–316.

Abdrabo, K. I., Saber, M., Kantoush, S. A., Elgharbawi, T., Sumi, T. & Elboshy, B. 2022b Applications of remote sensing for flood inundation mapping at urban areas in MENA region: Case studies of five Egyptian Cities. In: *Applications of Space Techniques on the Natural Hazards in the MENA Region* (Al Saud, M. M. ed.). Springer, Singapore, pp. 307–330.

Ahmed, O. E.-K. 2019 Are Arab cities prepared to face disaster risks? Challenges and opportunities. *Alexandria Engineering Journal* **58**, 479–486.

Bell, F. C. 1969 Generalized rainfall-duration-frequency relationships. *Journal of the Hydraulics Division ASCE* **95**, 311–327.

Bertrand-Krajewski, J. L. 2006 *Cours d'Hydrologie Urbaine: Modélisation des écoulements en réseau d'assainissement*. INSA de Lyon, France, p. 46.

Bisht, D. S., Chatterjee, C., Kalakoti, S., Upadhyay, P., Sahoo, M. & Panda, A. 2016 Modeling urban floods and drainage using SWMM and MIKE URBAN: A case study. *Natural Hazards* **84**, 749–776.

Boutaghane, H. B., Boulmaiz, T., Lameche, E. K., Lefkir, A., Hasbaia, M., Abdelbaki, C., Moulahoum, A. W., Keblouti, M. & Bermad, A. 2021 *Flood Analysis and Mitigation Strategies in Algeria*. DPRI Reports. Springer, Singapore. https://doi.org/10.1007/978-981-16-2904-4_3.

Brendel, C. E., Dymond, R. L. & Aguilar, M. F. 2021 Modeling storm sewer networks and urban flooding in Roanoke, Virginia, with SWMM and GSSHA. *Journal of Hydrologic Engineering* **26**, 05020044.

Bulti, D. T. & Abebe, B. G. 2020 A review of flood modeling methods for urban pluvial flood application. *Modeling Earth Systems and Environment* **6**, 1293–1302.

Chen, C. I. 1983 Rainfall intensity-duration-frequency formulas. *Journal of Hydraulic Engineering* **109** (12), 1603–1621.

Chocat, B. 1997 *Encyclopédie de l'hydrologie urbaine et de l'assainissement*. édition Hermès-Lavoisier, France.

Chocat, B. & Cabane, P. 1999 *Hydrologie urbaine: Modélisation et effet d'échelle*. La Houille Blanche, France, pp. 106–111.

Chow, V. T., Maidment, D. R. & Mays, L. W. 1988 *Applied Hydrology*. McGraw-Hill, New York, USA.

Dahm, C. N., Cleverly, J. R., Allred Coonrod, J. E., Thibault, J. R., Mcdonnell, D. E. & Gilroy, D. J. 2002 Evapotranspiration at the land/water interface in a semi-arid drainage basin. *Freshwater Biology* **47** (4), 831–843.

DHI 2017 *MOUSE Runoff Reference Manual*. DHI Water and Environment, Hørsholm, Denmark.

El Khalki, E. M., Tramblay, Y., Massari, C., Brocca, L., Simonneaux, V., Gascoin, S. & Saidi, M. E. M. 2020 Challenges in flood modeling over data-scarce regions: How to exploit globally available soil moisture products to estimate antecedent soil wetness conditions in Morocco. *Natural Hazards and Earth System Sciences* **20**, 2591–2607.

El-Kholei, A. O. 2019 Are Arab cities prepared to face disaster risks? Challenges and opportunities. *Alexandria Engineering Journal* **58**, 479–486.

Faridah, O., Lai, S. H. & Chang, K. B. 2013 RainIDF: Automated derivation of rainfall intensity–duration–frequency relationship from annual maxima and partial duration series. *Journal of Hydroinformatics* **15**, 1224–1233.

Farooq, Q. U. & Alluqmani, A. E. 2021 Application of soil based low impact development system for flash flood management of Jeddah, Saudi Arabia. *Journal of King Saud University – Engineering Sciences*. https://doi.org/10.1016/j.jksues.2021.09.006.

Gigović, L., Pamučar, D., Bajić, Z. & Drobnjak, S. 2017 Application of GIS-Interval rough AHP methodology for flood hazard mapping in urban areas. *Water* **9**, 360.

Hamlat, A., Kadri, C. B., Guidoum, A. & Bekkaye, H. 2021 Flood hazard areas assessment at a regional scale in M'zi wadi basin, Algeria. *Journal of African Earth Sciences* **182**, 104281.

Hemmati, M., Ellingwood, B. R. & Mahmoud, H. N. 2020 The role of urban growth in resilience of communities under flood risk. *EarthsFuture* **8** (3), e2019EF001382.

Hermoso, M., García-Ruiz, M. & Osorio, F. 2018 Efficiency of flood control measures in a sewer system located in the Mediterranean Basin. *Water* **10**, 1437.

Hettiarachchi, S., Wasko, C. & Sharma, A. 2017 Increase in urban flood risk resulting from climate change – The role of storm temporal patterns. https://doi.org/10.5194/hess-2017-352.

Hingray, B., Picouet, C. & Musy, A. 2014 *Hydrology, A Science For Engineers*. CRC press, Taylor and Francis Group, Boca Raton, FL.

Hosking, J. R. M. W. J. R. 1997 *Regional Frequency Analysis: An Approach Based on L-Moments*. Cambridge University Press, New York.

Kroll, S., Thoeye, C., De Gueldre, G., Van De Steene, B. & Willems, P. 2010 *A Semi Automated Simplification Method for Hydrodynamic Sewer Models*. NOVATECH, session 2.4.

Laborde, J. P. 2000 *Eléments d'hydrologie de surface*. L'Université de Nice-Sophia Antipolis, Edition Centre National de la Recherche Scientifique (C.N.R.S), France, p. 8137.

Lee, K.-S., Cho, W.-S., Hwang, J.-W., Byeon, S.-J. & Joo, K.-H. 2015 Numerical simulation for reducing the flood damage of green park using MIKE URBAN. *International Journal of Control and Automation* **8**, 37–54.

Lefebvre, G., Redmond, L., Germain, C., Palazzi, E., Terzago, S., Willm, L. & Poulin, B. 2019 Predicting the vulnerability of seasonally-flooded wetlands to climate change across the Mediterranean basin. *Science of the Total Environment* **692**, 546–555.

Loudyi, D. & Kantoush, S. A. 2020 Flood risk management in the Middle East and North Africa (MENA) region. *Urban Water Journal* **17**, 379–380.

Löwe, R., Urich, C., Domingo, N. S., Mark, O., Deletic, A. & Arnbjerg-Nielsen, K. 2017 Assessment of urban pluvial flood risk and efficiency of adaptation options through simulations – A new generation of urban planning tools. *Journal of Hydrology* **550**, 355–367.

Meylan, P. & Musy, A. 1999 *HYDROLOGIE FRÉQUENTIELLE EDITIONS*H*G*A**. Suisse, Bucarest. ISBN 978-2-88074-797-8.

Moriasi, D. N. G. M. W., Pai, N. & Daggupat, P. 2015 Hydrologic and water quality models: Performance measures and evaluation criteria. *Transactions of the ASABE* **58**, 1763–1785.

Morita, M. 2011 Quantification of increased flood risk due to global climate change for urban river management planning. *Water Science and Technology* **63**, 2967–2974. https://doi.org.10.2166/wst.2011.172.

Musy, A. & Higy, C. 2010 *Hydrology: A Science of Nature*. Taylor and Francis, New York.

Nguyen, T. T., Ngo, H. H., Guo, W. & Wang, X. C. 2020 A new model framework for sponge city implementation: Emerging challenges and future developments. *Journal of Environmental Management* **253**, 109689.

Nkwunonwo, U. C., Whitworth, M. & Baily, B. 2020 A review of the current status of flood modeling for urban flood risk management in the developing countries. *Scientific African* **7**, e00269.

Peña-Guzmán, C. A., Melgarejo, J., Prats, D., Torres, A. & Martínez, S. 2017 Urban water cycle simulation/management models: A review. *Water* **9**, 285.

Saber, M., Abdrabo, K. I., Habiba, O. M., Kantosh, S. A. & Sumi, T. 2020 Impacts of triple factors on flash flood vulnerability in Egypt: Urban growth, extreme climate, and mismanagement. *Geosciences* **10** (1), 24.

Salazar-Briones, C., Ruiz-Gibert, J. M., Lomelí-Banda, M. A. & Mungaray-Moctezuma, A. 2020 An integrated urban flood vulnerability index for sustainable planning in arid zones of developing countries. *Water* **12**, 608.

Sardou, M. M. S. & Missoum, H. 2016 Compilation of historical floods catalog of northwestern Algeria: First step towards an atlas of extreme floods. *Arabian Journal of Geosciences* **9**, 455.

Stefan, R., Gerald, K. & Dirk, M. 2021 *Poster_Hazard Assessment of Pluvial Flooding in Urban Areas Under Consideration of Fluvial Flooding*.

Talchabhadel, R. & Man Sharkya, N. 2015 Rainfall runoff modeling for flood forecasting (A case study on West Rapti watershed). *Journal of Flood Engineering* **6**, 53–61.

Tamiru, H. & Wagari, M. 2021 Machine-learning and HEC-RAS integrated models for flood inundation mapping in Baro River Basin, Ethiopia. *Modeling Earth Systems and Environment* **7**. https:/doi.org/10.1007/s40808-021-01175-8.

World Bank 2014 *The World Bank Annual Report 2014*. World Bank, Washington, DC.

Xu, T., Xie, Z., Jiang, F., Yangb, S., Deng, Z., Zhao, L., Wen, G. & Du, Q. 2023 Urban flooding resilience evaluation with coupled rainfall and flooding models: A small area in Kunming city, China as an example. *Water Science & Technology* **87** (11), 2820. doi:10.2166/wst.2023.149.

Youssef, A. M., Sefry, S. A., Pradhan, B. & Alfadail, E. A. 2015 Analysis on causes of flash flood in Jeddah city (Kingdom of Saudi Arabia) of 2009 and 2011 using multi-sensor remote sensing data and GIS. *Geomatics, Natural Hazards and Risk* **7**, 1018–1042.

Zahmatkesh, Z., Kumar Jha, S., Coulibaly, P. & Stadnyk, T. 2019 An overview of river flood forecasting procedures in Canadian watersheds. *Canadian Water Resources Journal/Revue Canadienne des Ressources Hydriques* **44**, 213–229.

Zhou, Q., Panduro, T. E., Thorsen, B. J. & Arnbjerg-Nielsen, K. 2013 Adaption to extreme rainfall with open urban drainage system: An integrated hydrological cost-benefit analysis. *Environmental Management* **51**, 586–601.